Science 18 Dec 2020:

Vol. 370, Issue 6523, pp. 1438-1442

DOI: 10.1126/science.aba5555

# Title: Relativistic Kinematics of a Magnetic Soliton

**Authors:** Lucas Caretta<sup>1</sup>, Se-Hyeok Oh<sup>2</sup>, Takian Fakhrul<sup>1</sup>, Dong-Kyu Lee<sup>3</sup>, Byung Hun Lee<sup>1</sup>, Se Kwon Kim<sup>4</sup>, Caroline A. Ross<sup>1</sup>, Kyung-Jin Lee<sup>2,3,5</sup>, and Geoffrey S. D. Beach<sup>1\*</sup>

#### **Affiliations:**

10

15

20

25

<sup>1</sup>Department of Materials Science and Engineering, Massachusetts Institute of Technology,

Cambridge, Massachusetts 02139, USA.

<sup>2</sup>Department of Nano-Semiconductor and Engineering, Korea University, Seoul 02841, Korea.

<sup>3</sup>Department of Materials Science and Engineering, Korea University, Seoul 02841, Korea.

<sup>4</sup>Department of Physics and Astronomy, University of Missouri, Columbia, MO 65211, USA.

<sup>5</sup>KU-KIST Graduate School of Converging Science and Technology, Korea University, Seoul 02841, Korea.

\*Correspondence to: gbeach@mit.edu

**Abstract:** A tenet of special relativity is that no particle can exceed the speed of light. In certain magnetic materials, the maximum magnon group velocity serves as an analogous relativistic limit for the speed of magnetic solitons. Here, we drive domain walls to this limit in a low-dissipation magnetic insulator using pure spin currents from the spin Hall effect. We achieve record current-driven velocities in excess of 4300 m/s, within  $\sim 10\%$  of the relativistic limit, and observe key signatures of relativistic motion associated with Lorentz contraction, leading to velocity saturation. The experimental results are well-explained through analytical and atomistic modeling. These observations provide critical insight into the fundamental limits of the dynamics of magnetic solitons and establish a readily-accessible experimental framework to study relativistic solitonic physics.

One Sentence Summary: Magnetic domain walls are driven to their relativistic speed limit, where the signatures of Lorentz contraction leading to velocity saturation are observed experimentally.

## **Main Text:**

5

10

15

20

In 1905, Einstein showed that Newtonian mechanics based on Galilean invariance breaks down at high speeds (1). Instead, Lorentz contraction and time dilation conspire to ensure that the velocity of an object never exceeds the speed of light c, irrespective of the reference frame of the observer. In certain condensed matter systems, such as dislocations in crystals (2), charge density waves (3) and magnetic domain walls (4–9), space and time variables are entangled in such a way that quasiparticle solitonic solutions of the equations of motion can likewise exhibit relativistic kinematics. For quasi-one-dimensional uniaxial magnetic systems at rest relative to the observer, this can be explicitly shown by describing low-energy dynamics within the Lagrangian formalism. Here, under the conditions of continuum theory, the Euler-Lagrange equation takes the form of the widely-studied Lorenz-invariant sine-Gordon equation (see Supplementary Information for complete derivation) (4–9),

$$\frac{\partial^2 \theta}{\partial t^2} - c_m^2 \frac{\partial^2 \theta}{\partial x^2} + \frac{c_m^2}{\Delta_0^2} \sin \theta = 0, \tag{1}$$

where  $\theta/2$  is the polar magnetization angle,  $c_m \equiv v_g^{max}$  is the maximum magnon group velocity, and  $\Delta_0$  is the characteristic magnetic lengthscale (the equilibrium domain-wall width). This model describes stationary states, where the azimuthal magnetization angle is constant in time, such that the magnetization dynamics can be simply described by just the polar angle  $\theta/2$  in Eq. (1). The sine-Gordon equation shown in Eq. (1) is invariant under the Lorentz transformation of the space (x) and time (t) variables through the Lorentz factor  $\gamma' = (1 - v^2/c_m^2)^{-1/2}$  with arbitrary velocity  $|v| < c_m$ , where  $c_m$  plays a role analogous to c in the theory of special relativity (5, 7-10). This relativistic nature of the field dynamics in Eq. (1) is naturally inherited by the dynamics of its nonlinear solitonic solution, a traveling magnetic domain wall (DW),  $\theta(x,t) =$ 

 $4 \tan^{-1} \left[ \exp \left( \frac{x - vt}{\Delta} \right) \right]$ , which behaves like a "relativistic" free extended particle whose velocity is ultimately limited by  $v_g^{max}$  (4, 5, 8, 9).

In real systems, DWs are typically driven by an external force and subjected to damping, which can be captured by including two terms on the right-hand side of the sine-Gordon equation,

$$\frac{\partial^2 \theta}{\partial t^2} - c_m^2 \frac{\partial^2 \theta}{\partial x^2} + \frac{c_m^2}{\Delta_0^2} \sin \theta = \tau^{-1} \frac{\partial \theta}{\partial t} + f \sin \frac{\theta}{2}, \tag{2}$$

where  $\tau$  is the relaxation time of the magnetic dynamics and f represents the driving force proportional to the applied field (see Supplementary Information for complete derivation). Although the damping term  $\propto \tau^{-1}$  breaks the Lorentz invariance of the equation, it has been shown numerically and analytically that the solution is still given by the same ansatz, such that a DW moving at the velocity v still exhibits relativistic-like effects (11–15) – that is, the length contraction of its width and the limitation of its velocity are governed by the Lorentz factor shown above. In particular, the equation of motion of the DW momentum mimics Newton's second law for a point particle (5), and thus the DW width  $\Delta_0$  and terminal DW velocity  $v_0 = (\gamma \Delta_0 / \alpha) H$ , transform to

$$\Delta = \Delta_0 \sqrt{1 - \left(v/v_g^{max}\right)^2} \tag{3}$$

and

5

10

15

$$v = v_0 \sqrt{1 - \left(v/v_g^{max}\right)^2} \tag{4}$$

in the laboratory frame (5, 8), where  $\gamma$  is the gyromagnetic ratio,  $\alpha$  is the Gilbert damping, and H is the driving field (see Supplementary Information). That is, Lorentz contraction of the DW width ensures that its velocity never exceeds  $v_g^{max}$  (4, 5, 8, 9). Equation (2), and its solution with

relativistic-like phenomena, hold for antiferromagnets, ferrimagnets, and ferromagnets. A

complete mapping of the sine-Gordon equation to these magnetic systems can be found in the

Supplementary Information.

5

10

15

20

In ferromagnets, large damping limits the DW mobility, and dynamical instabilities such

as Walker breakdown (16) typically set in far below the magnonic limit, making relativistic

kinematics inaccessible. However, in antiferromagnets and ferrimagnets, precessional dynamics is

suppressed (17–20) and the possibility of relativistic kinematics under experimentally-realizable

conditions has recently been predicted (12, 13, 15, 21–23). Here, we show that by using a low-

dissipation ferrimagnetic iron garnet, current-induced torques can drive DWs to record velocities

in excess of 4300 m/s, limited by Lorentz contraction of the DW width as v asymptotically

approaches the magnonic limit. Our experimental results are supported by analytical and atomistic

modeling of the dynamics, which account well for our observations. These results give critical

insights into the ultimate speed of magnetic quasiparticle excitations, and hence the operating

speed of spintronic devices that utilize them(24, 25), while providing a new arena for relativistic

solitonic physics that puts related phenomena such as THz spin-wave radiation (15, 23) within

experimental reach.

We examined DW dynamics in 6.9 nm thick epitaxial Bi-substituted yttrium iron garnet

(BiYIG, Fig. 1a; see Methods), a perpendicularly-magnetized ferrimagnetic insulator with low

damping (26) to facilitate a high DW mobility. A thin Pt overlayer was used to generate a current-

induced torque via the spin Hall effect (27–29), which has recently been shown to allow for

current-induced switching and fast DW motion in rare earth iron garnets (30–32). Figure 1b shows

exemplary x-ray diffraction results that illustrate fully strained film growth with high structural

quality. Perpendicular magnetic anisotropy with near-bulk saturation magnetization was

10

15

20

confirmed with vibrating sample magnetometry (VSM) and polar magneto-optical Kerr effect measurements (MOKE, Fig. 1c; see Methods and Supplementary Information). Deterministic magnetization switching via the spin Hall effect (Fig. 1d) was verified by injecting current pulses in a lithographically-fabricated track (see Methods). The switching polarity depends on the direction of a longitudinal bias field (Fig. 1d), as expected for damping-like spin-orbit torque (SOT).

Current-induced DW motion was imaged in a conventional racetrack geometry (Fig. 2a) using a wide-field MOKE microscope (Methods). The track had electrical contacts at either end for current injection and an orthogonal Au strip line for initializing DWs via an Oersted field from a short current pulse. Spin current injected from Pt via the spin Hall effect exerts a torque on a DW that is maximum when the moments in the DW are collinear with the charge current density  $\mathbf{j}$  (Néel DW), and which vanishes when the DW moments are orthogonal to  $\mathbf{j}$  (Bloch DW) (33, 34). We observe no current-induced motion in the absence of an in-plane bias field along  $\mathbf{j}$ , which implies that the equilibrium DW orientation is fully Bloch, as also evidenced by an independent measurement (see Supplementary Information). This is in contrast to recent reports in thulium iron garnet, in which Néel DWs were observed as a result of a significant Dzyaloshinskii-Moriya interaction (DMI) (31, 32). Therefore, DMI is evidently negligibly small or absent in our non rare-earth-containing BiYIG. However, a longitudinal bias field  $H_x$  can be used to induce a Néel character in the DWs, such that spin Hall current-driven motion can be realized, as seen in Fig. 2d.

In a one-dimensional model, DW motion driven by a magnetic field can be described by  $v = (\gamma \Delta / \alpha) H$  (34). This can be readily adapted to SOT-driven DW motion by modeling the current-driven torque as an effective magnetic field  $H_{\rm eff}$  driving the DW. In particular, for a ferrimagnet with strongly exchanged-coupled antiparallel sublattices, such as BiYIG, and in the

10

15

20

absence of DMI, the velocity expression takes the following analytical form in the standard onedimensional model:

$$v = \frac{\pi \gamma_{\text{eff}} \Delta}{2 \alpha_{\text{eff}}} \frac{\mu_0 H_{\text{eff}}}{\sqrt{1 + [H_{\text{eff}} / (\alpha_{\text{eff}} H_Y)]^2}}.$$
 (5)

where  $\mu_0$  is the vacuum permeability. This expression resembles the case for SOT-driven ferromagnets (33, 34); however, the gyromagnetic ratio  $\gamma$  and Gilbert damping  $\alpha$  are rescaled to  $\gamma_{\rm eff} = \frac{M_S}{S}$  and  $\alpha_{\rm eff} = \frac{S_\alpha}{S}$  (where  $S_\alpha$  is the magnetic dissipation) to account for the net angular momentum S of the antiferromagnetically-coupled sublattices in the ferrimagnet (18) (see Methods). Here, the current-induced effective field  $H_{\rm eff} \propto j$  accounts for the combined dampinglike torque exerted on each of the individual sublattices, ultimately driving the DW motion. The torque drives both sublattice DWs in the same direction dictated by the DW chirality and the injected spin polarization direction. BiYIG lacks magnetic ions on the dodecahedral sites and hence does not show compensation. Nonetheless, this model accounts for ferrimagnetic currentdriven dynamics irrespective of the degree of compensation, as shown theoretically (35) and experimentally (18). Away from angular momentum compensation, as is the case for BiYIG, the dynamics exhibits two distinct regimes: a low-drive regime, with  $v \propto j$ , and a high-drive regime, where the velocity saturates toward  $v_{\rm sat} = \frac{\pi}{2} \gamma \Delta \mu_0 H_x$ . The latter saturation of the velocity occurs because, with increasing j, the SOT drives the DW further and further towards the Bloch configuration where it is less susceptible to the torque. This is the origin of the denominator in Eq. 5, which leads to an asymptotic velocity limit proportional to the field  $H_x$  that defines the "stiffness" of the Néel orientation.

Figure 2e shows measured v(j) curves for several  $H_x$ . In all cases, v first increases with j and then saturates, consistent with the dynamics described above. Low damping contributes to a

10

15

20

high mobility which, together with a small critical current of  $\sim 5 \times 10^{10}$  A/m², allows for high speeds to be achieved at modest current densities. Under small in-plane fields,  $v_{\rm sat}$  scales linearly with  $H_{\rm x}$  (Fig. 2f), as expected from Eq. 5. However, at larger  $H_{\rm x}$ , a ceiling is reached, beyond which further stiffening of the DW fails to increase  $v_{\rm sat}$ . This observation is the central experimental result of this work. All conventional velocity-limiting mechanisms relate to the strength of the restoring torque in the DW when it is driven away from its equilibrium orientation. Our observation of a limiting velocity that is independent of the stiffness of the DW, that is, independent of the internal energetics of the DW itself, has never before been observed experimentally. This indicates that the observed velocity maximum arises from a more fundamental limiting phenomenon. Similar measurements were performed on a thinner garnet film GSGG/BiYIG(2.4 nm)/Pt(4.0 nm) are shown in the Supplementary Information and yield consistent, velocity saturation results.

To shed light on the observed DW velocity saturation and magnon dynamics, we perform Brillouin light scattering (BLS) on an exemplary, fully-strained GSGG/BiYIG(29 nm) film. A 532 nm laser is incident on the sample under an applied  $H_x$  (Fig. 3a; see Methods), where inelastic scattering of incident photons from magnons under momentum and energy conservation can yield quantitative magnetic information about the film. Figure 3b shows the BLS results at an incident angle of  $\theta = 45^{\circ}$  for various  $H_x$ . The three observed peaks were analyzed based on a model of dipole-exchange spin wave dispersion relations in thin films (36) (see Supplementary Information). To identify the magnon modes of these peaks, we measured spectra at various angles of incidence ( $\theta$ , see Fig. 3c). The different wavevector (k) sensitivty of each mode allows us to identify the first BLS spectrum peak as the Damon-Eshbach (DE) mode and the third peak as the perpendicular standing spin wave (PSSW; see Supplementary Information) [REF]. Note that the second peak which is independent of  $H_x$ , is a phonon peak [REF]. The PSSW mode along film

10

15

20

thickness yields the maximum exchange contribution (37, 38) and enables the extraction of the exchange constant of the thin film (39). From the  $H_x$ - and k-dependence of the BLS spectra (Figs. 3b,c), we obtain  $A = (4.54 \pm 0.40) \times 10^{-12} J/m$  for 29 nm BiYIG film. Wihin error, the extracted value is comparable with the bulk BiYIG exchange constant,  $4.15 \times 10^{-12} J/m$  (40), signifying that the exchange constrant of fully strained, epitaxial BiYIG films does not vary from bulk and is relatively thickness-independent.

The spin wave dispersion relation in a strongly exchange-coupled ferrimagnet is given by (15)

$$\omega_{\pm} = \frac{\pm \delta_s + \sqrt{\delta_s^2 + 4\rho(Ak^2 + K)}}{2\rho} \tag{6}$$

where  $\omega$  is the angular frequency, '+' and '-' represent spin wave solutions with opposite handedness, k is the wavevector, A is the exchange constant,  $\delta_s$  is the net spin density, K is the easy-axis anisotropy, and  $\rho$  is the inertia of the dynamics (see Methods and Supplementary Information). Figure 4a shows the spin-wave dispersion relation and group velocity calculated using the experimental material parameters for our BiYIG film (see Supplementary Information for details of experimentally-measured parameters), including the BLS-confirmed exchange constant. From Eq. (6), expect a maximum group velocity  $v_g^{max} \approx 5000$  m/s. The maximum observed DW velocity is ~4300 m/s, significantly faster than that seen in compensated rare earth-transition metal alloys driven by field or current (17, 18). This velocity is comparable to  $v_g^{max}$ , suggesting that the theory for full relativistic kinematics should be employed to properly describe the observed DW dynamics.

Since the saturation velocity of v(j) scales as  $v_{sat} = \frac{\pi}{2} \gamma \Delta \mu_0 H_x$ , the deviation from linearity between  $v_{sat}$  and  $H_x$  at high speeds in Fig. 2f is consistent with a reduction in the dynamical DW

10

15

20

width  $\Delta$  from its static value,  $\Delta_0$ . By estimating  $\Delta_0$  from  $v_{sat}$  at small  $H_x$  (see Supplemental Information),  $\Delta/\Delta_0$  can be inferred directly from the dynamics data, since any unknown parameters are eliminated in the ratio. In Fig. 4b, we see that  $\Delta/\Delta_0$  is indeed reduced at high speeds, suggesting that Lorentz contraction gives rise to the asymptotic velocity maximum in Fig. 2f.

Figures 4c,d show analytical and atomistic modeling that fully account for the experimental observations. Equation (4) can be readily rearranged to yield an analytical expression for the relativistic DW velocity in a one-dimensional model. Specifically, for the case of ferrimagnets, the DW dynamics manifest as

$$v = \frac{\tilde{v}}{\sqrt{1 + \left[\tilde{v}/v_g^{max}\right]^2}},\tag{7}$$

where we have replaced  $v_0$  in Eq. (4) with  $\tilde{v}(j; H_x)$ , the SOT-driven DW velocity given by Eq. 5 with the equilibrium DW width  $\Delta_0$  used. Figure 4c shows analytically-computed v(j) curves for various  $H_x$ , using all experimentally-determined material parameters, including the exchange constant, Gilbert damping, applied magnetic fields, and effective fields (see Supplemental Information). Figure 4d shows the corresponding  $v_{\text{sat}}$  versus  $H_x$ . We have also performed two-sublattice atomistic simulations of the current-driven motion for a one-dimensional ferrimagnetic system, using atomistic parameters corresponding to the continuum material parameters used in the analytical model, all of which were experimentally measured (see Methods and Supplementary Information). We find excellent agreement between the analytical model and the full atomistic simulations, as seen in Figs. 4c,d, with deviations arising primarily from the fact that finite  $H_x$  changes the equilibrium DW width  $\Delta_0$ , which is not captured in the analytical model. The dynamical DW width extracted from the atomistic simulations closely follows the expected

Lorentz contraction, as seen in Fig. 4b. A comparison with the results in Figs. 2e,f shows that this

modeling fully captures the experimentally-observed behavior. We hence conclude that Lorentz

contraction as v approaches  $v_q^{max}$  serves as the underlying cause of the velocity ceiling observed

in Figs. 2f and 4d.

5

10

15

In summary, we demonstrate current-driven DW motion in perpendicularly magnetised

BiYIG, with velocities exceeding 4300 m/s, limited by a saturation velocity that is independent

of the Néel stiffness of the DW. These exceptionally high DW velocities further illustrate the utility

of iron garnets in spintronic devices. We show that at these speeds, relativistic kinematics leads to

this experimentally-observed velocity limit, which can be understood as a consequence of Lorentz

contraction of the DW width rooted in Lorentz invariance of the underlying equations of motion.

Our results provide critical insight into the dynamical behavior of DWs at ultrafast velocities, and

demonstrate that magnetic systems under suitable conditions can serve as a laboratory platform

for the relativistic kinematics of solitons. This may further enable the experimental observation of

rare relativistic phenomena such as soliton dynamics in two- or three-dimensional systems such as

skyrmions under well-controlled conditions, and of solitons interacting dynamically with the

lattice structure that is expected to mimic general relativity to a certain degree.

#### **References and Notes:**

5

10

- 1. A. Einstein, Zur Elektrodynamik bewegter Körper. Ann. Phys. 4, 891–921 (1905).
- 2. F. C. Frank, J. H. van der Merwe, One-dimensional dislocations. I. Static theory. *Proc. R. Soc. London.* **198**, 205–216 (1949).
- 3. M. J. Rice, A. R. Bishop, J. A. Krumhansl, S. E. Trullinger, Weakly pinned fröhlich charge-density-wave condensates: A new, nonlinear, current-carrying elementary excitation. *Phys. Rev. Lett.* **36**, 432–435 (1976).
- 4. J. F. Currie, Aspects of exact dynamics for general solutions of the sine-Gordon equation with applications to domain walls. *Phys. Rev. A.* **16**, 1692–1699 (1977).
- 5. M. B. Fogel, S. E. Trullinger, A. R. Bishop, J. A. Krumhansl, Dynamics of sine-Gordon solitons in the presence of perturbations. *Phys. Rev. B.* **15**, 1578–1592 (1977).
- 6. H. J. Mikeska, Solitons in a one-dimensional magnet with an easy plane. *J. Phys. C Solid State Phys.* **11**, L29 (1978).
- 7. K. M. Leung, D. Hone, D. L. Mills, P. S. Riseborough, S. E. Trullinger, Solitons in the linear-chain antiferromagnet. *Phys. Rev. B.* **21**, 4017–4026 (1980).
  - 8. A. R. Bishop, W. F. Lewis, A theory of intrinsic coercivity in narrow magnetic domain wall materials . *J. Phys. C Solid State Phys.* **12**, 3811–3825 (1979).
  - 9. K. A. Long, A. R. Bishop, Nonlinear excitations in classical ferromagnetic chains. *J. Phys. A Math. Gen.* **12**, 1325–1339 (1979).
    - 10. D. I. Paul, Soliton theory and the dynamics of a ferromagnetic domain wall. *J. Phys. C Solid State Phys.* **12**, 585–593 (1979).

- 11. H. How, R. C. Ohandley, F. R. Morgenthaler, Soliton theory for realistic magnetic domain-wall dynamics. *Phys. Rev. B.* **40**, 4808–4817 (1989).
- 12. S. K. Kim, Y. Tserkovnyak, O. Tchernyshyov, Propulsion of a domain wall in an antiferromagnet by magnons. *Phys. Rev. B.* **90**, 104406 (2014).
- 5 O. Gomonay, T. Jungwirth, J. Sinova, High Antiferromagnetic Domain Wall Velocity Induced by Néel Spin-Orbit Torques. *Phys. Rev. Lett.* **117**, 017202 (2016).
  - T. Shiino, S.-H. Oh, P. M. Haney, S.-W. Lee, G. Go, B.-G. Park, K.-J. Lee,
     Antiferromagnetic Domain Wall Motion Driven by Spin-Orbit Torques. *Phys. Rev. Lett.* 117, 087203 (2016).
- S.-H. H. Oh, S. K. Kim, D.-K. K. Lee, G. Go, K.-J. J. Kim, T. Ono, Y. Tserkovnyak, K.-J.
   J. Lee, *Phys. Rev. B*, in press, doi:10.1103/PhysRevB.96.100407.
  - 16. N. L. Schryer, L. R. Walker, The motion of 180° domain walls in uniform dc magnetic fields. *J. Appl. Phys.* **45**, 5406–5421 (1974).
- K.-J. J. Kim, S. S. K. Kim, Y. Hirata, S.-H. H. Oh, T. Tono, D.-H. H. Kim, T. Okuno, W.
   S. Ham, S. S. K. Kim, G. Go, Y. Tserkovnyak, A. Tsukamoto, T. Moriyama, K.-J. J. Lee,
   T. Ono, Fast domain wall motion in the vicinity of the angular momentum compensation temperature of ferrimagnets. *Nat. Mater.* 16, 1187–1192 (2017).
  - 18. L. Caretta, M. Mann, F. Büttner, K. Ueda, B. Pfau, C. M. Günther, P. Hessing, A. Churikova, C. Klose, M. Schneider, D. Engel, C. Marcus, D. Bono, K. Bagschik, S. Eisebitt, G. S. D. Beach, Fast current-driven domain walls and small skyrmions in a compensated ferrimagnet. *Nat. Nanotechnol.* 13, 1154–1160 (2018).
    - 19. S. Yang, K. Ryu, S. Parkin, Domain-wall velocities of up to 750 m s 1 driven by

Science 18 Dec 2020:

Vol. 370, Issue 6523, pp. 1438-1442

DOI: 10.1126/science.aba5555

exchange-coupling torque in synthetic antiferromagnets. *Nat. Nanotech.* **10**, 221–226 (2015).

- S. A. Siddiqui, J. Han, J. T. Finley, C. A. Ross, L. Liu, Current-Induced Domain Wall Motion in a Compensated Ferrimagnet. *Phys. Rev. Lett.* 121, 057701 (2018).
- 5 21. D. Bouzidi, H. Suhl, Motion of a Bloch domain wall. *Phys. Rev. Lett.* **65**, 2587–2590 (1990).
  - 22. M. Yan, C. Andreas, A. Kákay, F. García-Sánchez, R. Hertel, Fast domain wall dynamics in magnetic nanotubes: Suppression of Walker breakdown and Cherenkov-like spin wave emission. *Appl. Phys. Lett.* **99**, 122505 (2011).
- T. Shiino, S.-H. Oh, P. M. Haney, S.-W. Lee, G. Go, B.-G. Park, K.-J. Lee,
   Antiferromagnetic Domain Wall Motion Driven by Spin-Orbit Torques. *Phys. Rev. Lett.* 117, 087203 (2016).
  - 24. S. S. P. Parkin, M. Hayashi, L. Thomas, Magnetic domain-wall racetrack memory. *Science*. **320**, 190–4 (2008).
- 15 25. A. Fert, V. Cros, J. Sampaio, Skyrmions on the track. *Nat. Nanotechnol.* **8**, 152–156 (2013).
  - L. Soumah, N. Beaulieu, L. Qassym, C. Carrétéro, E. Jacquet, R. Lebourgeois, J. Ben Youssef, P. Bortolotti, V. Cros, A. Anane, Ultra-low damping insulating magnetic thin films get perpendicular. *Nat. Commun.* 9, 3355 (2018).
- 27. I. M. Miron, K. Garello, G. Gaudin, P.-J. Zermatten, M. V. Costache, S. Auffret, S. Bandiera, B. Rodmacq, A. Schuhl, P. Gambardella, Perpendicular switching of a single ferromagnetic layer induced by in-plane current injection. *Nature.* **476**, 189–193 (2011).

- 28. L. Liu, C.-F. Pai, Y. Li, H. W. Tseng, D. C. Ralph, R. A. Buhrman, Spin-Torque Switching with the Giant Spin Hall Effect of Tantalum. *Science* (80-.). **336**, 555–558 (2012).
- 29. S. Woo, M. Mann, A. J. Tan, L. Caretta, G. S. D. Beach, Enhanced spin-orbit torques in Pt/Co/Ta heterostructures. *Appl. Phys. Lett.* **105**, 212404 (2014).
- C. O. Avci, A. Quindeau, C.-F. Pai, M. Mann, L. Caretta, A. S. Tang, M. C. Onbasli, C. A. Ross, G. S. D. Beach, Current Induced Switching in a Magnetic Insulator. *Nat. Mater.* 16, 309–314 (2017).
- 31. C. O. Avci, E. Rosenberg, L. Caretta, F. Büttner, M. Mann, C. Marcus, D. Bono, C. A.

  Ross, G. S. D. Beach, Interface-driven chiral magnetism and current-driven domain walls in insulating magnetic garnets. *Nat. Nanotechnol.* **14**, 561–566 (2019).
  - 32. S. Vélez, J. Schaab, M. S. Wörnle, M. Müller, E. Gradauskaite, P. Welter, C. Gutgsell, C. Nistor, C. L. Degen, M. Trassin, M. Fiebig, P. Gambardella, High-speed domain wall racetracks in a magnetic insulator. *Nat. Commun.* **10**, 4750 (2019).
- 15 33. E. Martinez, S. Emori, N. Perez, L. Torres, G. S. D. Beach, Current-driven dynamics of Dzyaloshinskii domain walls in the presence of in-plane fields: Full micromagnetic and one-dimensional analysis. *J. Appl. Phys.* **115**, 213909 (2014).
  - 34. A. Thiaville, S. Rohart, É. Jué, V. Cros, A. Fert, Dynamics of Dzyaloshinskii domain walls in ultrathin magnetic films. *Europhys. Lett.* **100**, 57002 (2012).
- 20 35. E. Martínez, V. Raposo, Ó. Alejos, Current-driven domain wall dynamics in ferrimagnets: Micromagnetic approach and collective coordinates model. *J. Magn. Magn. Mater.* **491**, 165545 (2019).

10

15

- 36. S. O. Demokritov, B. Hillebrands, A. N. Slavin, Brillouin light scattering studies of confined spin waves: Linear and nonlinear confinement. *Phys. Rep.* **348** (2001), pp. 441–489.
- 37. K. Matsumoto, T. Brächer, P. Pirro, T. Fischer, D. Bozhko, M. Geilen, F. Heussner, T. Meyer, B. Hillebrands, T. Satoh, Optical determination of the exchange stiffness constant in an iron garnet. *Jpn. J. Appl. Phys.* **57** (2018), doi:10.7567/JJAP.57.070308.
- 38. O. Gaier, J. Hamrle, S. Trudel, B. Hillebrands, H. Schneider, G. Jakob, Exchange stiffness in the Co2FeSi heusler compound. *J. Phys. D. Appl. Phys.* **42**, 40–43 (2009).
- 39. O. Gaier, J. Hamrle, S. Trudel, A. Conca Parra, B. Hillebrands, E. Arbelo, C. Herbort, M. Jourdan, Brillouin light scattering study of Co2Cr0.6Fe 0.4Al and Co2FeAl Heusler compounds. *J. Phys. D. Appl. Phys.* **42** (2009), doi:10.1088/0022-3727/42/8/084004.
  - 40. A. P. Malozemoff, J. C. Slonczewski, *Magnetic domain walls in bubble materials* (Academic Press, 1979).
- 41. T. Fakhrul, S. Tazlaru, L. Beran, Y. Zhang, M. Veis, C. A. Ross, Magneto-Optical Bi:YIG Films with High Figure of Merit for Nonreciprocal Photonics. *Adv. Opt. Mater.* 7, 1900056 (2019).
  - 42. S. K. Kim, K. J. Lee, Y. Tserkovnyak, Self-focusing skyrmion racetracks in ferrimagnets. *Phys. Rev. B.* **95**, 140404 (2017).
- 43. S. H. Oh, K. J. Lee, Ferrimagnetic domain wall motion induced by damping-like spin-orbit torque. *J. Magn.* **23**, 196–200 (2018).
- J. F. K. Cooper, C. J. Kinane, S. Langridge, M. Ali, B. J. Hickey, T. Niizeki, K. Uchida,E. Saitoh, H. Ambaye, A. Glavic, Unexpected structural and magnetic depth dependence

Science 18 Dec 2020:

20

Vol. 370, Issue 6523, pp. 1438-1442

DOI: 10.1126/science.aba5555

of YIG thin films. Phys. Rev. B. 96, 104404 (2017).

- A. Mitra, O. Cespedes, Q. Ramasse, M. Ali, S. Marmion, M. Ward, R. M. D. Brydson, C.
   J. Kinane, J. F. K. Cooper, S. Langridge, B. J. Hickey, Interfacial Origin of the
   Magnetisation Suppression of Thin Film Yttrium Iron Garnet. Sci. Rep. 7, 11774 (2017).
- 5 46. S. M. Suturin, A. M. Korovin, V. E. Bursian, L. V Lutsev, V. Bourobina, N. L. Yakovlev, M. Montecchi, L. Pasquali, V. Ukleev, A. Vorobiev, A. Devishvili, N. S. Sokolov, Role of gallium diffusion in the formation of a magnetically dead layer at the Y3Fe5O12/Gd3Ga5O12 epitaxial interface. *Phys. Rev. Mater.* 2, 104404 (2018).
- 47. L. Caretta, E. Rosenberg, F. Büttner, T. Fakhrul, P. Gargiani, M. Valvidares, Z. Chen, P. Reddy, D. A. Muller, C. A. Ross, G. S. D. Beach, Interfacial Dzyaloshinskii-Moriya interaction arising from rare-earth orbital magnetism in insulating magnetic oxides. *Nat. Commun.* 11, 1090 (2020).
- 48. S. Emori, E. Martinez, K.-J. J. Lee, H.-W. W. Lee, U. Bauer, S.-M. M. Ahn, P. Agrawal, D. C. Bono, G. S. D. Beach, Spin Hall torque magnetometry of Dzyaloshinskii domain walls. *Phys. Rev. B.* **90**, 4427 (2014).
  - 49. S. Emori, D. C. Bono, G. S. D. Beach, Interfacial current-induced torques in Pt/Co/GdOx. *Appl. Phys. Lett.* **101**, 042405 (2012).
  - 50. F. D. M. Haldane, Nonlinear field theory of large-spin Heisenberg antiferromagnets:

    Semiclassically quantized solitons of the one-dimensional easy-axis Néel state. *Phys. Rev. Lett.* **50**, 1153–1156 (1983).
    - 51. I. V. Bar'yakhtar, B. A. Ivanov, Dynamic solitons in a uniaxial antiferromagnet. *Sov. Phys JETP.* **58**, 190–197 (1984).

15

20

- 52. V. Baltz, A. Manchon, M. Tsoi, T. Moriyama, T. Ono, Y. Tserkovnyak, Antiferromagnetic spintronics. *Rev. Mod. Phys.* **90**, 015005 (2018).
- 53. N. L. Schryer, L. R. Walker, The motion of 180° domain walls in uniform dc magnetic fields. *J. Appl. Phys.* **45**, 5406–5421 (1974).
- 5 54. B. A. Ivanov, A. L. Sukstanskii, Three-dimensional solitons in ferrites and their stability. *Solid State Commun.* **50**, 523–527 (1984).
  - 55. D. Loss, D. P. DiVincenzo, G. Grinstein, Suppression of tunneling by interference in half-integer-spin particles. *Phys. Rev. Lett.* **69**, 3232–3235 (1992).
  - 56. A. Altland, B. Simons, *Condensed Matter Field Theory* (Cambridge University Press, 2006).
  - 57. H. Goldstein, C. Poole, J. Safko, *Classical mechanics* (Addison-Wesley, Boston, 2002).
  - 58. E. U. Die dynamik der Blochschen wand. Helv. Phys. Acta. 37, 245 (1964).

Acknowledgments: Devices were fabricated using equipment in the MIT Microsystems Technology Laboratory. This work made use of the MIT Materials Research Science and Engineering Center (MRSEC) Shared Experimental Facilities, supported by the National Science Foundation under award number DMR-1419807. The authors thank L. Liu for use of the ion milling equipment. L.C. acknowledges financial support from the NSF Graduate Research Fellowship Program and from the GEM Consortium. The authors thank Felix Büttner, Jason Bartell, and Boris Ivanov for helpful discussions. **Funding:** This work was supported by the DARPA TEE program and SMART, an nCORE Center. K.J.L. was supported by Samsung Research Funding Center of Samsung Electronics under project no. SRFCMA1702-02. S.K.K.

10

15

20

25

30

was supported by the start-up fund at the University of Missouri. Author contributions: L.M.C., C.A.R., and G.S.D.B. conceived the project and planned the experiments; T.F. synthesized and characterized BiYIG films. L.M.C. performed vibrating sample magnetometry, L.M.C. deposited the metal layers and micro-fabricated the domain wall tracks; L.M.C. prepared the experimental setup; L.M.C. performed the domain wall measurements; Numerical modeling was performed by S.H.O. and D.K.L. B.H.L. performed Brillouin light scattering experiments and analysis. Analytical modeling was performed by K.J.L, S.K.K., G.S.D.B, and L.M.C.. L.M.C. and G.S.D.B. wrote the manuscript with input from S.K.K, K.J.L., and C.A.R. All authors contributed to the discussion of the data in the manuscript and Supplementary Information. Competing interests: Authors declare no competing financial interests. Data and materials availability: The data supporting the findings of this study are available within the paper and other findings of this study are available from the corresponding author upon reasonable request.

# **Supplementary Materials**

Materials and Methods

Growth, Characterization and Patterning of Materials

Magneto-optical Kerr effect (MOKE) Measurements

Domain wall track current injection

Effective Scaling Model for Ferrimagnetic Dynamics

Spin-wave dispersion and maximum group velocity calculation

Numerical Atomistic Modeling

Brillouin Light Scattering Spectroscopy

Magnetic Property Characterization

Measurement of spin Hall efficiency,  $\chi$  and effective spin Hall angle,  $\theta_{eff}$ 

 $\Delta(H_x)$  Domain wall broadening correction

Displacement as a function of pulse width

Measurement of the exchange constant from Brillouin light scattering (BLS)

Mapping of the low-energy dynamics of uniaxial magnets to the sine-Gordon equation

Antiferromagnets with easy-axis anisotropy

Antiferromagnetically-coupled ferrimagnets with easy-axis anisotropy

Ferromagnets with easy-axis anisotropy

Fig S1 - S6

References (40 - 59)

### **Figures**

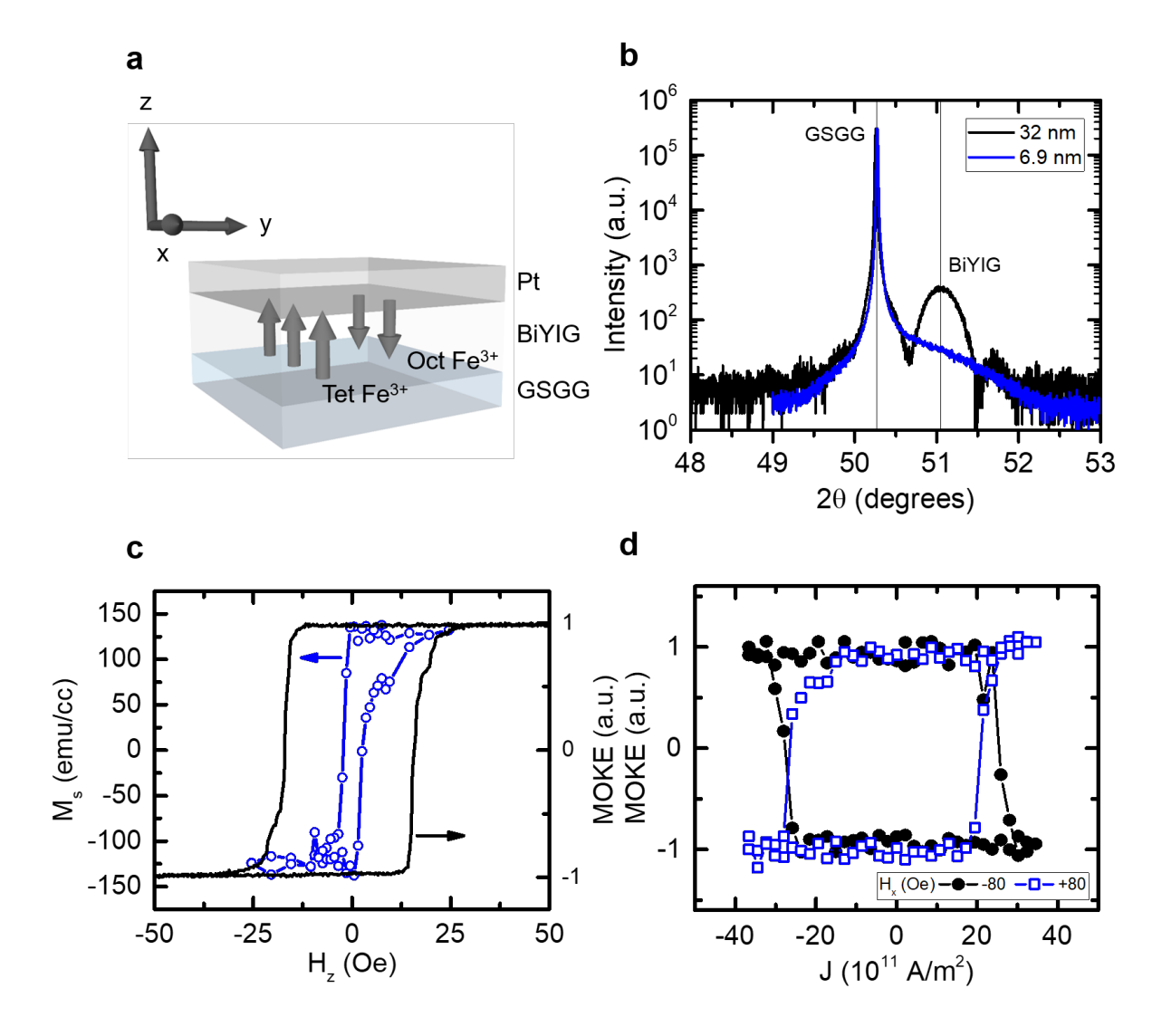


Figure 1| Structural and magnetic characterisation. a. Schematic of GSGG/BiYIG/Pt trilayer structure. Arrows indicate the orientation of the Fe<sup>3+</sup> magnetic moments in BiYIG where Tet (Oct) stands for the tetragonal (octahedral) site. b. High-resolution X-ray diffraction ( $2\theta - \omega$  scan) of 32 nm thick (black) and 6.9 nm thick (blue) GSGG/BiYIG. c. Vibrating sample magnetometry (blue, left axis) and magneto-optical Kerr effect (MOKE, black, right axis) hysteresis loops of a perpendicularly magnetised GSGG/BiYIG(6.9 nm) film. d. Current-induced switching probed via MOKE in GSGG/BiYIG(6.9 nm)/Pt(4.0 nm).  $M_s$ , saturation magnetisation. a.u., arbitrary units.

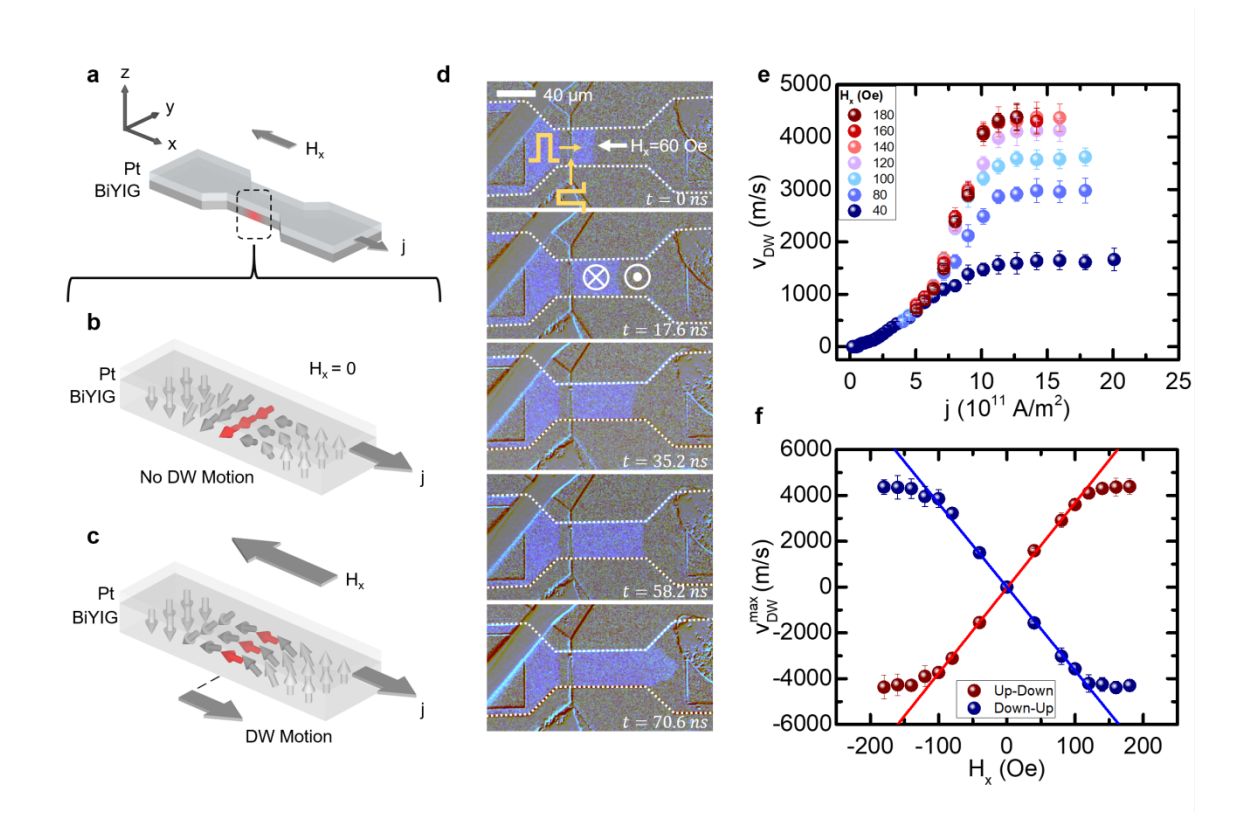


Figure 2| Relativistic domain wall motion. a. Schematic of the domain wall track structure of BiYIG(6.9 nm)/Pt(4.0 nm). The light grey overlayer represents the Pt layer. Red color in BiYIG represents a nucleated domain wall. A zoomed-in view of the domain wall is shown in **b**. for the case of no applied in-plane field  $H_x$ , and **c**. under a significant in-plane field. Arrows indicate the orientation of net magnetisation. **d**. Time stamped magneto-optical Kerr microscopy depicting current-driven domain wall motion in BiYIG. A train of pulses with current density  $j \sim 1.65 \times 10^{12} A m^{-2}$  was injected between each image frame. **e**. Domain wall velocity  $v_{DW}$  as a function of j for various  $H_x$ . **f**. Saturation velocity  $v_{DW}^{max}$  as a function of  $H_x$ . Error bars represent the standard deviation of three independent measurements of the domain wall velocity.

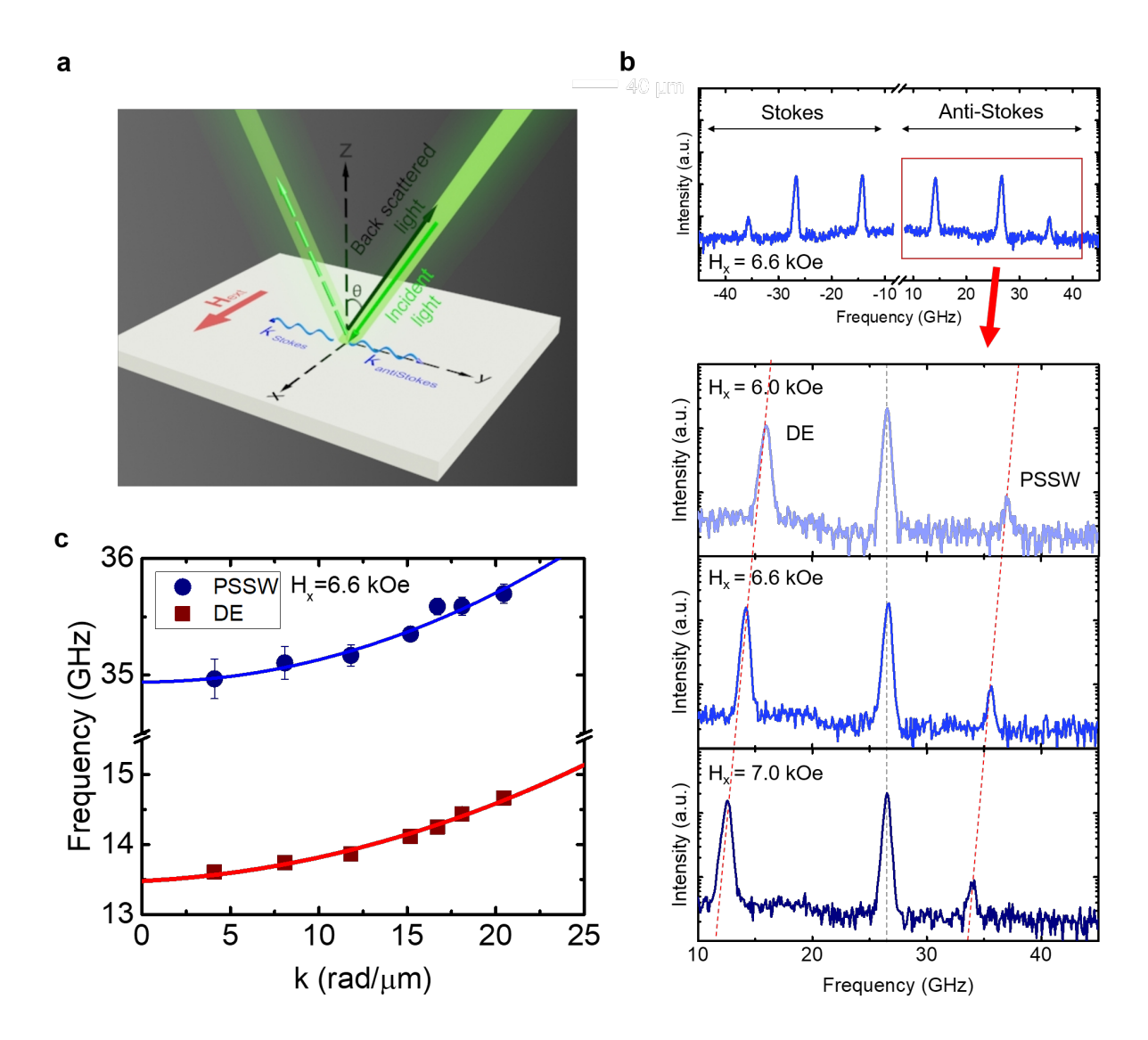


Figure 3| Brillouin light scattering. a. Schematic of BLS spectroscopy. Thermally excited spin waves at room temperature were detected by BLS signals with an in-plane  $H_x$ . b. BLS spectra of GSGG/BiYIG(29 nm) for various in-plane fields  $H_x$  at an incident angle of  $45^0$  ( $k = 16.7 \, rad \cdot \mu m^{-1}$ ). The top spectra shows both Stokes and Anti-Stokes peaks, while subsequent spectra detail the Anti-Stokes peaks. Red dotted lines track the Damon-Eshbach (DE) and and perpendicular standing spin wave (PSSW) mode peaks. c. Dependence of the frequency on wavevector k at  $H_x = 6.6 \, kOe$ . Solid lines are fitted curve using spin wave dispersion relations of each DE and

PSSW mode. (see Supplementary Information). Error bars in (c) are fit uncertainty of the BLS spectra peaks.

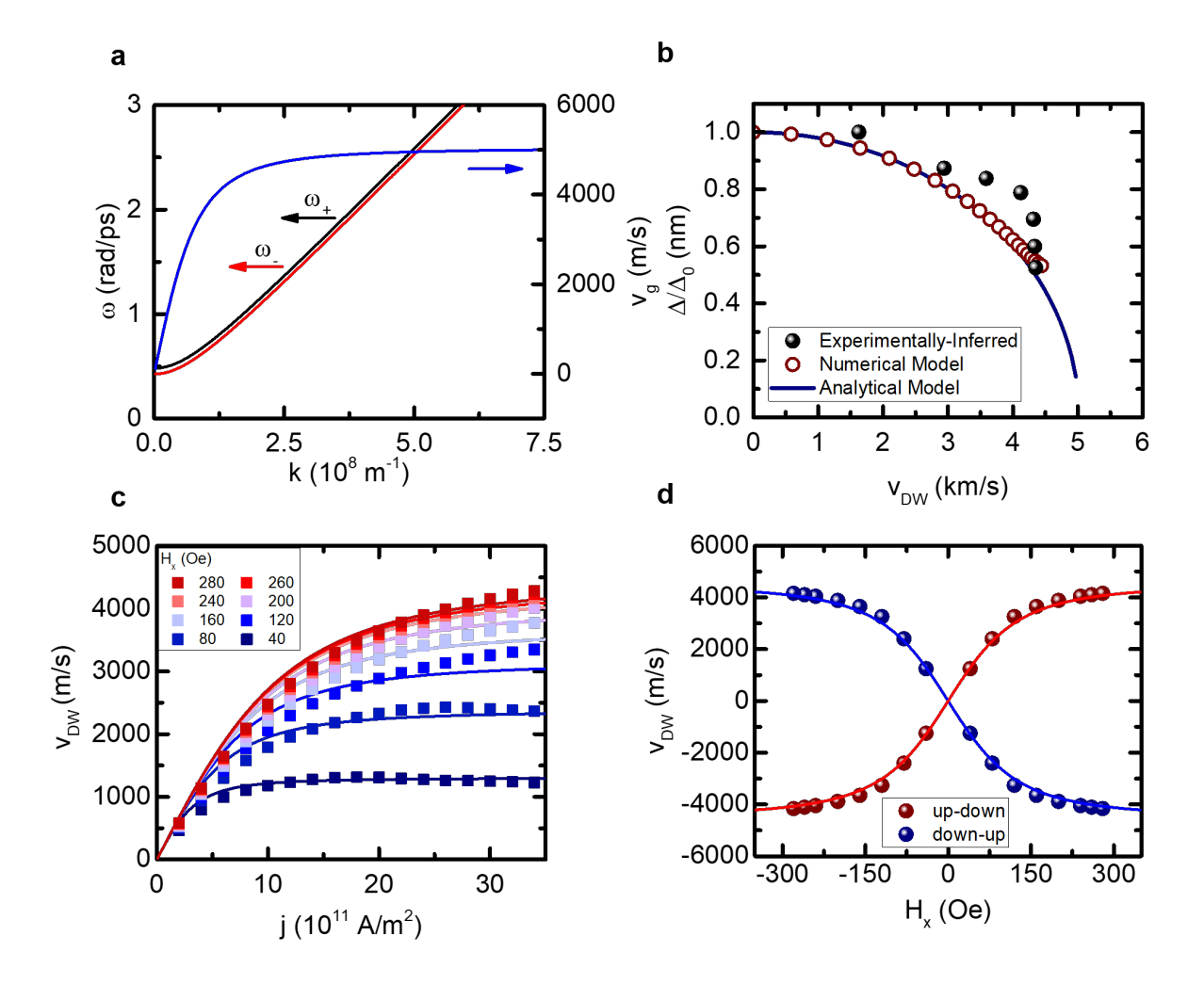


Figure 4 Modeling of relativistic domain-wall motion. a. Analytically computed dispersion relations (Eq. 6) of spin waves of each handedness and their common group velocity in BiYIG(6.9 nm). Lorentz contraction of the normalized domain wall width GSGG/BiYIG(6.9 nm)/Pt(4.0 nm) calculated analytically (lines, Eq. 3), through atomistic simulations (open circles), and experimentally-inferred from the domain wall velocity data (orbs). **c.** Analytical (lines, Eq. 7) and atomistic (symbol) modeling of the domain wall velocity  $v_{DW}$  as a function of current density j for various in-plane fields  $H_x$ . d. Analytical (lines, Eq. 7) and atomistic (symbols) modeling of the saturation velocity  $v_{DW}^{max}$  as a function of  $H_x$ . k, wave vector.  $\omega$ , frequency of spin wave.